

## STRUCTURE AND MECHANICS OF THE SQUID MANTLE

PATRICK S. MACGILLIVRAY<sup>1</sup>, ERIK J. ANDERSON<sup>1</sup>, GLENDA M. WRIGHT<sup>2</sup> AND M. EDWIN DEMONT<sup>1,\*</sup>

<sup>1</sup>Biology Department, St Francis Xavier University, PO Box 5000, Antigonish, Nova Scotia, Canada B2G 2W5 and

<sup>2</sup>Department of Anatomy and Physiology, Atlantic Veterinary College, University of Prince Edward Island, 550 University Avenue, Charlottetown, Prince Edward Island, Canada C1A 4P3

\*Author for correspondence (e-mail: edemont@stfx.ca)

Accepted 21 December 1998; published on WWW 17 February 1999

### Summary

The goal of this study was to obtain a complete description of the elastic modulus and hysteresis of the mantle tissue of the squid *Loligo pealei* over the entire functional region of the mantle. In addition, *in vivo* strains were measured to allow calculations of the amount of energy stored and returned in each region of the mantle studied, and microscopic analysis of the tissue was carried out with the aim of correlating macroscopic properties with microscopic structure. The results of dynamic tissue tests indicate that mean elastic moduli for each of the 35 mantle positions tested ranged from  $5.0 \times 10^5$  to  $1.2 \times 10^6 \text{ Nm}^{-2}$ . The elastic modulus varied within a narrow range, in no predictable manner. Mean hysteresis values for each position varied from 19.7% to 27.3% with no discernible patterns found either around

or along the mantle. *In vivo* mantle strains peaked in the middle (lengthwise) of the mantle and declined towards both ends, and the absolute strains increased with increasing swimming velocity. Energy storage calculations showed that most energy was stored in the middle of the mantle, with an increase in storage with increased swimming velocity. Microscopic tissue analysis found direct correlations between macroscopic properties and microscopic characteristics, and electron microscopical analysis of all three types of intramuscular fibre revealed that all three types are collagenous in nature.

Key words: mantle, muscle, elastic modulus, hysteresis, energy storage, swimming, squid, *Loligo pealei*, locomotion, collagen.

### Introduction

Squids, soft-bodied animals whose skeletal support is derived from a musculo-hydrostatic system, are remarkable animals in that they can swim as well as many fish, but they do so using jet propulsion (Gosline and DeMont, 1985). For example, *Todarus pacificus*, the Japanese squid, can swim continuously for 2.5 months at an average speed of  $0.3 \text{ m s}^{-1}$  ( $0.9$  body lengths  $\text{s}^{-1}$ ) covering a migratory distance of 2000 km (Gosline and DeMont, 1985). For short escape bursts, however, squids have been recorded swimming at  $3 \text{ m s}^{-1}$ , and some larger species are believed to swim three times as fast.

The locomotor system of the squid produces the fastest locomotion known in aquatic invertebrates and generates the highest hydrostatic pressures measured in any animal (Ward and Wainwright, 1972). The squid mantle is chiefly composed of a mass of circular muscle fibres, divided in a more or less regular way into rectangular blocks by thin partitions of radial muscle fibres (Bone et al., 1981). These radial muscle fibres are not continuous around the mantle, but only run for a few millimetres. The mantle is not divided into regular rings of circular muscle by these partitions, but rather the partitions interdigitate, and the thickness of the rings varies. Two different types of circular muscle fibre exist in the mantle (Mommensen et al., 1981). The circular muscles are made up of a thick central layer of fast-twitch fibres making up more than

80% of the total circular muscle volume. These muscles are characterized by a sparse capillary bed and fibres with very small mitochondrial cores. Two thin layers of slow-twitch, aerobic fibres, characterized by a rich vascular bed and fibres with central mitochondrial cores, occupy the other portion of the fibre volume (Bone et al., 1981). The radial muscle fibres have the same characteristics as muscle fibres of the central core and are composed entirely of fast-twitch, glycolytic muscle fibres. These muscle fibres insert on an inner and outer layer of robust collagen fibres (the inner and outer tunics, respectively).

There is a second system of collagenous fibres, which runs through the thickness of the mantle muscle tissue in several different orientations (Gosline and Shadwick, 1983a). One set of these intramuscular fibres (IM-1) can be seen in longitudinal sections of the mantle (Fig. 1A) running from the outer tunic to the inner tunic, at an angle of approximately  $30^\circ$  relative to the long axis of the animal (Ward and Wainwright, 1972). In sections cut tangentially to the surface of the mantle (Fig. 1B), these fibres do not run parallel to the long axis but at a small angle ( $\approx 10\text{--}15^\circ$ ) relative to this axis (Bone et al., 1981), thus following a steep 'spiral' through the muscle tissue. A second set of intramuscular fibres (IM-2) can be seen in transverse sections that pass through layers of radially oriented muscles

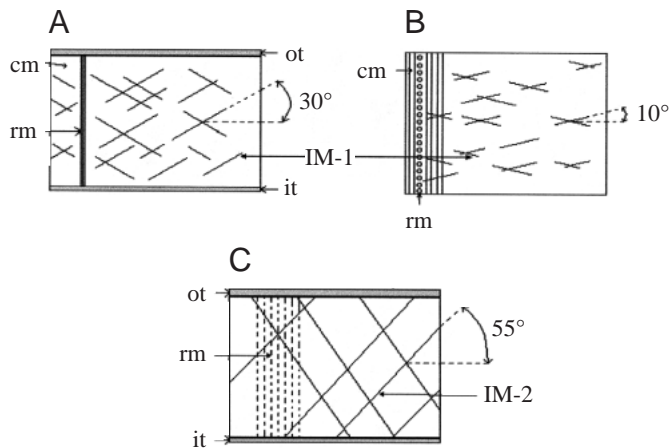


Fig. 1. The organization of intramuscular fibres in the squid mantle. (A) In longitudinal sections, the fibres in system IM-1 are seen to run from the outer tunic to the inner tunic at an angle of approximately  $30^\circ$  relative to the long axis. (B) In sections cut tangential to the mantle surface, the fibres in IM-1 run at an angle of  $10\text{--}15^\circ$  relative to the long axis. (C) In transverse sections through a layer of radial muscle, the fibres of IM-2 can be seen running from the outer tunic to the inner tunic at an angle of  $55^\circ$  relative to the surface of the mantle. ot, outer tunic; it, inner tunic; cm, circular muscle; rm, radial muscle (adapted from Gosline and Shadwick, 1983a).

(Fig. 1C). These fibres also run from the outer tunic to the inner tunic and are oriented at approximately  $55^\circ$  relative to the mantle surface. They are confined to the planes of the radial muscle bands (Bone et al., 1981). The fibres in both the inner and outer tunics and in IM-1 and IM-2 all appear to follow very straight paths. There is, however, a third set of intramuscular fibres (IM-3) that can be seen running parallel to the circular muscles. These fibres are not straight but appear coiled or buckled.

The fibres of the inner and outer tunics can be identified as collagen, but the intramuscular fibres have not yet been identified definitively. Gosline and Shadwick (1983a) report that the fibres in IM-1 are highly birefringent and exhibit the same birefringence as that observed for rat tail tendon collagen fibres (Aaron and Gosline, 1980). In addition, they were not able to measure the birefringence of the fibres in systems IM-2 and IM-3 since these fibres are only seen in sections that run parallel to a set of muscle fibres, resulting in a strong birefringence of the myofibrils which masks that of the connective tissue fibres (Gosline and Shadwick, 1983a). Bone et al. (1981) report that some of the intramuscular fibres, as well as those forming the major overlapping layers of the thick outer tunic, stain with three different histological stains that are characteristic of elastin fibres.

The jet cycle of a squid has been carefully analyzed by simultaneously recording the electromyographic (EMG) activity of squid mantle muscles, changes in mantle cavity pressure and changes in mantle diameter (Gosline et al., 1983). Three distinguishable phases of activity occur in the full jet cycle. The first phase, hyperinflation, occurs at the start of the

jet cycle. The mantle begins at some intermediate resting diameter and the jet cycle is initiated with a period of hyperinflation, powered by contractions of the radial muscles. Hyperinflation functions to fill the mantle cavity maximally, allowing a more powerful jet to follow. The second phase is the jet. Immediately following hyperinflation, the circular muscles contract, expelling the sea water in the mantle cavity and creating the jet. The third phase involves the refilling of the mantle. After the jet, the mantle re-expands to its resting diameter. This expansion is probably powered largely by the elastic recoil of the connective tissue fibre lattice (intramuscular fibres). Thus, in this 'basic' pattern of escape jetting, the major role of the radial muscles is primarily during the hyperinflation phase. However, it is likely that there is a certain amount of variation in this basic pattern, as the animals used were significantly restrained (Gosline et al., 1983). Cephalopods, with their highly developed complex nervous systems (Wells, 1978), are probably capable of several different patterns of muscle activity.

The bulk of the muscle in the squid mantle seems to be active only during the high-speed bursts involved in an escape response, and the radial muscles have no role in refilling the mantle when the squid is swimming slowly. During slow swimming, the refilling process is powered by an elastic mechanism composed of the intramuscular fibres embedded throughout the mantle.

The intramuscular fibres are stretched reversibly by approximately 10% during the jet cycle (Gosline and DeMont, 1985). During this process, the fibres can store and release large amounts of elastic energy. When the circular muscles contract during the jet phase, the mantle wall thickens and the first two sets of fibres (IM-1 and IM-2) are stretched. In mechanical studies of these tissue springs, Gosline and Shadwick (1983b) found that the fibres store energy efficiently, releasing approximately 75% of it when they relax. Energy from these springs is then used to power the expansion of the mantle during refilling. In a similar manner, the third set of fibres (IM-3) is stretched when the radial muscles contract during hyperinflation, and the energy stored is released when the radial muscles relax at the start of the jet phase. During maximal escape jets, both the elastic system antagonizing the circular muscles and the elastic system antagonizing the radial muscles are used, presumably to maximize power output during escape responses (Gosline et al., 1983).

The goal of the present study was to obtain a complete description of mantle tissue mechanics in the squid *Loligo pealei* over the entire functional region of the mantle. In addition, *in vivo* strains occurring in the swimming squid were measured, to allow estimates of the amount of energy stored and returned in each area of the mantle studied. Quantitative microscopic analysis of all regions of the mantle tested mechanically were carried out to attempt to correlate the macroscopic properties of the mantle with its microscopic characteristics. This study is part of a larger project that will integrate the tissue and fluid mechanics in order to calculate all *in vivo* forces on swimming squid. This approach was used

previously to examine *in vivo* forces on a swimming scallop (Cheng et al., 1996; Cheng and DeMont, 1996a,b, 1997).

**Materials and methods**

Specimens of *Loligo pealei* (LeSueur) were obtained from the Marine Resources Center of the Marine Biological Laboratory (MBL), Woods Hole, MA, USA. The squid were captured either by a common jigging method from nearby wharves or by the MBL trawler. Animals were maintained in running sea water of ambient temperature (approximately 10 °C). Specimens were killed by decapitation after having

been anaesthetized by lowering their body temperature to 0 °C. Squid used in this study had mantle lengths within the range 22–25 cm.

The sampling strategy utilized was designed to measure the physical properties over the entire functional region of the mantle. Tissue ‘rings’ were taken sequentially along the length of the mantle (Fig. 2A) and labelled as  $0.90X_m$ ,  $0.75X_m$ ,  $0.60X_m$ ,  $0.45X_m$  and  $0.30X_m$ , where  $X_m$  is mantle length from the posterior mantle apex (Fig. 2A) to the anterior mantle apex. Posterior and anterior here and throughout the text refer to the functional anterior (head) and posterior ends. Within a particular ring, rectangular tissue blocks were removed from seven locations around the circumference of the ring (Fig. 2B). This sampling method resulted in a total of 35 sampling positions. Blocks were cut as shown in Fig. 2C, with the circumferential dimension ( $c$ ) of the specimen being only slightly greater than the mantle thickness ( $t$ ) to prevent buckling of the sample (Gosline and Shadwick, 1983a).

Tissue blocks of length ( $l$ ) approximately 0.007 m and thickness varying from 2 to 5 mm were magnified (10×), and the dimensions were measured using a dissecting microscope and video dimension analyzer (VDA). Tissue blocks were mounted in the apparatus shown in Fig. 3. A moveable top plate applied a compressive strain to the circumferential dimension ( $c$ ) which replicated an *in vivo* compression. The top plate was attached to a Cambridge 300B lever system, which could apply any displacement while measuring the force required to maintain the strain. A Hewlett Packard 8904A multifunction synthesizer produced a sinusoidal signal whose midline strain amplitude could be adjusted by using the lever system. These instruments were used to apply a pre-determined strain to the tissue and to oscillate the tissue sinusoidally from rest to this desired strain. Both the voltage signal controlling the displacement and the voltage signal corresponding to the force were collected on a Hewlett Packard digitizing oscilloscope and stored on a computer. LabVIEW and

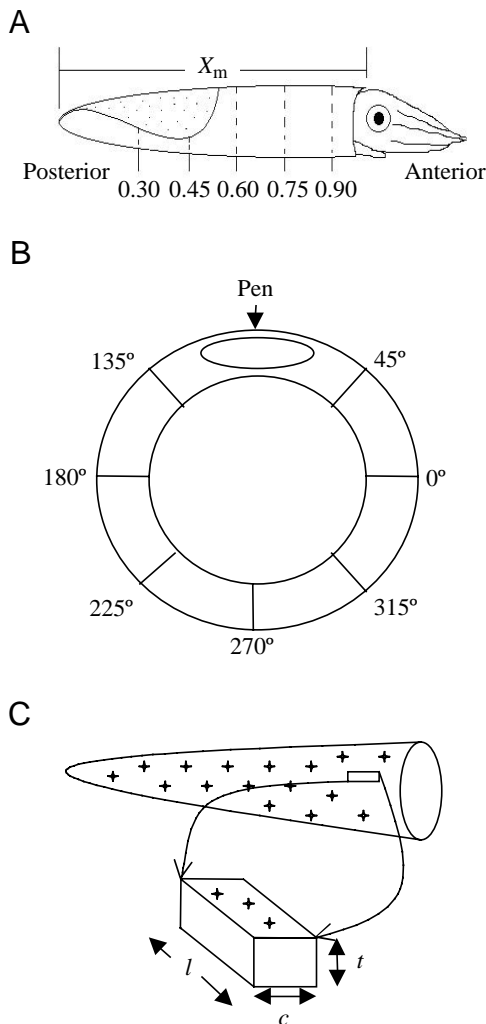


Fig. 2. The location and orientation of mantle samples. (A) The samples were taken from five tissue rings along the length of the mantle.  $X_m$  is the mantle length from the posterior mantle apex to the anterior mantle apex. Each of the five longitudinal positions represents a percentage of this mantle length, i.e.  $0.30X_m$  represents 30% of  $X_m$ . (B) Within a ring, seven angular sampling locations were used around the circumference. These positions are defined looking down the mantle towards the posterior end of the squid. (C) The dimensions of the tissue blocks cut from these positions within a ring and their orientation relative to the surrounding mantle tissue are shown.  $l$ , length;  $c$ , circumferential dimension;  $t$ , thickness.

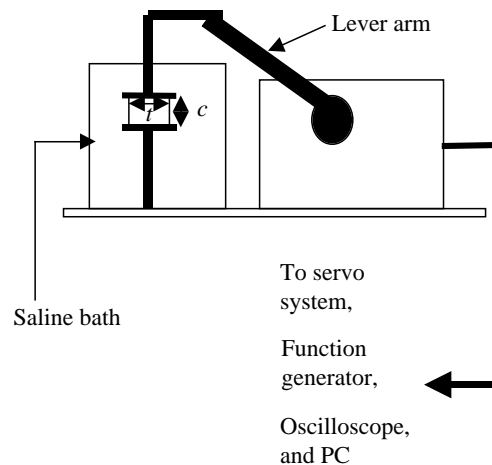


Fig. 3. Schematic diagram showing the mechanical testing and data-collection apparatus.  $c$ , sample circumferential dimension;  $t$ , sample thickness.

MATLAB software were used for both data acquisition and analysis.

Initial estimates of *in vivo* circumferential strain were measured from high-speed video recordings of casual jetting *Loligo pealei* taken using a Redlake Motionscope 500 high-speed camera at a frame rate of 125–250 frames s<sup>-1</sup>. The squid were filmed in flumes at the Woods Hole Oceanographic Institute (WHOI). If the volume of the mantle tissue is constant and the mantle length does not change significantly (Gosline and Shadwick, 1983a), the circumferential strain  $\epsilon_c$  can be calculated as:

$$\epsilon_c = 1 - \frac{R_f - \frac{t_f}{2}}{R_i - \frac{t_i}{2}}, \quad (1)$$

where  $R_f$  is the outer radius of the contracted squid,  $R_i$  is the resting outer radius,  $t_i$  is the resting thickness of the mantle (measured *post mortem*) and  $t_f$  is the thickness of the contracted mantle calculated using the formula:

$$t_f = R_f - \sqrt{R_f^2 - t_i(2R_i - t_i)}. \quad (2)$$

The initial estimate of *in vivo* circumferential strain was -14.5%, where negative values indicate compression. Since this circumferential strain was estimated from a casually jetting squid, it could be predicted that a squid undertaking escape-jetting muscle contractions would undergo a tissue strain of approximately -20% or greater. Thus, a maximum strain of -20% was chosen to be applied to the tissue. Swimming frequencies of filmed squid ranged from 0.4 Hz (slow casual jetting) to 0.9 Hz (fast casual jetting).

Initially, tissue blocks were tested to determine the temporal window available after death for mechanical tests to be made before *rigor mortis* set in and changed the properties of the tissue. The oscillation frequency began at 0.2 Hz and progressed to 1.1 Hz, increasing by increments of 0.1 Hz only after a complete set of force/displacement data for a cycle of loading and unloading had been recorded by the computer for each frequency. This range of frequencies was chosen to span the observed swimming frequencies.

The *rigor mortis* test trials revealed that the tissue modulus remained the same for at least 3 h after death if the tissue was kept immersed in sea water of ambient temperature. This window led to the procedure of testing only one 'ring' from each squid killed. This procedure took approximately 2 h from the time of death to the end of testing of the last block of tissue. Tissue rings from 15 squid were used and, when pooled, yielded three 'full sets' of sampling data for each location. The force/displacement data recorded by the computer from the mechanical testing were converted to stress/strain data using the formulae:

$$\sigma = \frac{F}{A}, \quad (3)$$

$$\epsilon = \frac{\Delta c}{c}, \quad (4)$$

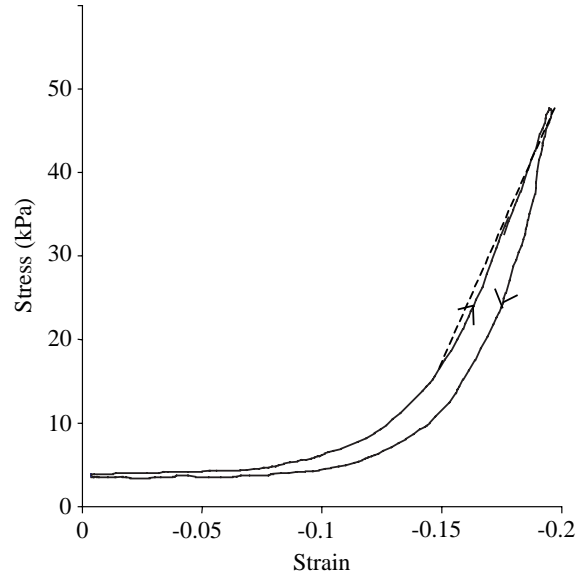


Fig. 4. A stress/strain curve resulting from a single loading/unloading cycle of a squid mantle tissue block (longitudinal position  $0.45X_m$ , where  $X_m$  is mantle length, angular position  $180^\circ$ , see Fig. 2; frequency of oscillation 0.7 Hz). The line drawn on the figure at a tangent to the curve represents the slope used to determine the elastic modulus of the tissue.

where  $\sigma$  is stress (Pa),  $F$  is force (N),  $A$  is cross-sectional area onto which the force is applied (m<sup>2</sup>),  $\epsilon$  is strain (%),  $\Delta c$  is the change in the circumferential dimension of the sample, and  $c$  is the resting circumferential dimension of the sample.

Stress and strain were calculated and plotted for each trial frequency using the tissue sample dimensions (Fig. 4). The non-zero stress at zero strain is simply an artefact of the experimental procedure, which required lowering the compressive plate to a location which just caused deformation. The hysteresis of the tissue (the percentage of energy put into the tissue upon loading which is lost and not returned upon unloading) was calculated by taking the area between the loading and unloading curves, and the elastic modulus was calculated by taking the slope of the curve between the strains -0.15 and -0.19. The elastic modulus and hysteresis value were calculated for each frequency of oscillation from 0.2 Hz to 1.0 Hz for each sample, for all three full rounds of samples.

The statistical analysis methods available in Microsoft Excel 97 were utilized to carry out an extensive statistical analysis on the elastic modulus values. Initially, a regression analysis of modulus against frequency of oscillation was performed for data from each of the 35 positions. Next, single-factor analyses of variance (ANOVAs) were performed on samples tested from the same position on different squid to determine whether their modulus means were significantly different from each other. Following this, single-factor ANOVAs were carried out for all samples taken from an individual squid to determine whether the tissue samples from around the tissue ring were significantly different. Since statistical differences were found, Tukey tests were performed for all samples taken from the

same ring to determine exactly which of the position moduli differed significantly from each other. After this, correlation analyses were carried out to determine whether the modulus varied with certain variables (see Fig. 2C) such as the thickness of the tissue sample ( $t$ ), the transverse area of the sample ( $t \times l$ ), the tunic area of the sample ( $c \times l$ ) and the circumferential dimension of the sample ( $c$ ). An identical statistical analysis procedure was carried out for the hysteresis values.

The video sequences used to estimate the circumferential strain were later intensively analyzed. From digitized images, the instantaneous outer mantle diameter was measured along the length of the mantle. The maximum circumferential strain ( $\epsilon_c$ ) at each  $X_m$  position was calculated using equations 1 and 2. Recordings of three casually jetting squid travelling at different velocities were analyzed, and the maximum circumferential strain at each of the five  $X_m$  positions was determined for two distinct contractions for each squid, giving two (one for each of the two separate contractions analyzed) complete maximum strain distributions (a strain distribution meaning strains for all five  $X_m$  positions) for each of the three squid. One of these squid had a swimming velocity of  $25 \text{ cm s}^{-1}$ , a speed that it could maintain for more than 2 h. The other two squid were travelling at higher swimming velocities of  $38\text{--}39 \text{ cm s}^{-1}$  which, on the basis of observations of squid swimming in the flume, is near the upper limit of prolonged swimming. The strains for the slow-swimming squid were used to produce a strain distribution for that swimming velocity, while the circumferential strain values for the fast-swimming squid were averaged to produce a strain distribution for a high-velocity squid.

Three whole squid were fixed in 10% formalin immediately after death and used for further tissue analysis. One squid mantle was cut into sections and put through a defatting procedure (Winkelmann and Schmitt, 1957). Tissue blocks from all 35 sampling positions were then removed from this squid and embedded in Tissue-Tek OCT compound (Miles Inc.) and frozen in a freezing microtome set at  $-20^\circ\text{C}$ . Transverse frozen sections  $40 \mu\text{m}$  thick were cut using this microtome, placed on slides and protected with coverslips. These slides were then viewed under a Leitz Laborlux 12 polarizing microscope ( $10\times$  magnification) under cross-polarized light. Beginning at the outer tunic, images were digitized using a Backman Vidcon camera linked to an IMAQ PCI-1408 frame grabber. Successive images from outer tunic to inner tunic were taken (varying from three to seven images depending on the thickness of the mantle). Two complete sections (one section being a set of images spanning outer tunic to inner tunic) from each of the 35 positions were digitized and stored on computer.

The polarized micrographs then were studied using quantitative image analysis. For each micrograph, radial muscle spacing (and thus circular muscle thickness), radial muscle thickness and the number of radial muscles were measured.

Samples of mantle from four squid were prepared for light and electron microscopy. Tissues for light microscopy were

fixed in Bouin's fluid for 24 h, washed and stored in 70% ethanol prior to being dehydrated in a graded series of ethanols, cleared in xylene and embedded in Tissue Prep (Fischer Scientific). Serial transverse and longitudinal sections,  $6 \mu\text{m}$  thick, were mounted on glass slides and stained using a modified Weigert's technique for demonstrating elastic, elaunin and oxytalan fibres (Montes, 1992). Positive controls for elastic, elaunin and oxytalan fibre staining consisted of sections of rat aorta collected from lean female Zucker rats *Rattus norvegicus* (Charles River, St Constant, Quebec, Canada), as described previously (Davidson et al., 1995).

Mantle samples collected from the middle region of the mantle (approximately  $0.60X_m$ ) were fixed for electron microscopy in 3% glutaraldehyde in  $0.1 \text{ mol l}^{-1}$  cacodylate buffer at pH 7.3 containing 10% sucrose for 24 h at room temperature ( $20^\circ\text{C}$ ). Samples were rinsed in  $0.1 \text{ mol l}^{-1}$  cacodylate buffer containing 10% sucrose, post-fixed in 1%  $\text{OsO}_4$  in cacodylate buffer at room temperature ( $20^\circ\text{C}$ ), then washed in buffer, dehydrated in an ethanol series and embedded in Spurr's resin. Sections ( $0.5 \mu\text{m}$  thick) were stained with 1% Toluidine Blue in 1% borax and examined to assess the orientation of the tissue. Ultrathin sections stained with uranyl acetate and lead citrate were examined and photographed using a Hitachi H600 or H7000 electron microscope operated at 75 kV. The dimensions of structures were measured from 20 representative samples of that structure in at least five micrographs at magnifications ranging from  $41\ 100\times$  to  $100\ 660\times$ .

## Results

Table 1 gives the mean elastic modulus values for each of the 35 mantle positions (note that  $1 \text{ N m}^{-2} = 1 \text{ Pa}$ ). Fig. 5 shows graphically the modulus values for all 35 mantle positions. Regression analysis carried out on the modulus data for each tissue sample to investigate frequency effects revealed that 31 out of 35 tests had  $F > F_{\text{crit}}$  (i.e. no significant linear relationship amongst modulus values for the different frequencies tested on a sample,  $P \leq 0.05$ ). Single-factor ANOVAs performed on samples tested from the same position to determine whether they were significantly different yielded 33 out of 35 sample positions having  $F > F_{\text{crit}}$  (i.e. sample means within each position are significantly different). Single-factor ANOVAs performed for all samples taken from each individual squid yielded 15 out of 15 tests with  $F > F_{\text{crit}}$  (i.e. all sample means within a tissue ring are not equal). Tukey tests carried out for all samples taken from the same ring to determine exactly which position moduli differed significantly from which yielded no discernible patterns from test to test. Correlation analyses performed for modulus/thickness of sample, modulus/transverse area of sample, modulus/tunic area of sample and modulus/circumferential dimension of sample all yielded extremely low correlations that were not significant.

Table 2 gives the mean hysteresis values for each of the 35 mantle positions Fig. 6 shows graphically the hysteresis values for all 35 mantle positions. Regression analysis carried out on

Table 1. Mean elastic modulus (MPa) for each position on the squid mantle

Ring position	Mantle position					Mean
	0.3X <sub>m</sub>	0.45X <sub>m</sub>	0.6X <sub>m</sub>	0.75X <sub>m</sub>	0.9X <sub>m</sub>	
0	0.735±0.057	0.613±0.028	0.962±0.064	0.586±0.056	0.699±0.076	0.719
45	0.916±0.088	0.774±0.035	0.504±0.032	0.911±0.122	0.854±0.074	0.792
135	0.985±0.086	0.768±0.037	0.985±0.086	0.942±0.113	0.947±0.029	0.925
180	0.669±0.025	0.641±0.027	0.878±0.087	0.632±0.077	0.853±0.023	0.734
225	0.831±0.045	0.104±0.072	0.104±0.142	0.867±0.079	0.819±0.051	0.919
270	1.2±0.145	0.124±0.045	0.974±0.051	0.694±0.100	0.824±0.038	0.985
315	0.928±0.095	0.108±0.045	0.82±0.045	0.685±0.062	0.767±0.099	0.856
Mean	0.894	0.879	0.880	0.760	0.823	

Mantle positions are defined in Fig. 2; X<sub>m</sub>, mantle length. Values are means ± s.e.m. (N=15) and are given as MPa.

the hysteresis data for each tissue sample to investigate frequency effects revealed that 30 out of 35 tests had *F* values that were not significant. Single-factor ANOVAs performed on samples tested from the same position yielded 28 out of 35 sample positions having  $F > F_{crit}$ . Single-factor ANOVAs performed on all samples taken from each squid revealed 15 out of 15 tests with  $F > F_{crit}$ . Tukey tests performed for all samples taken from the same ring yielded no discernible patterns from test to test. Correlation analysis carried out for hysteresis/thickness of sample, hysteresis/transverse area of sample, hysteresis/tunic area of sample and hysteresis/circumferential dimension of sample all yielded extremely low correlations that were not significant.

The maximum *in vivo* circumferential strain data for the slow-swimming squid are shown in Fig. 7A. The mean *in vivo* strain is maximal between 0.45 and 0.75X<sub>m</sub>, with the peak occurring at 0.60X<sub>m</sub>. The *in vivo* circumferential strain data for the two fast-swimming squid are shown in Fig. 7B, indicating a significant strain increase relative to the slow-swimming squid and a similar strain pattern with the peak strain again at 0.60X<sub>m</sub>.

Ten stress/strain loading curves representative of those recorded for all mantle positions were used in a LabVIEW program which determined the area under the curves up to a specified strain and then averaged these values to calculate the energy stored per unit volume (=energy input) at each of the

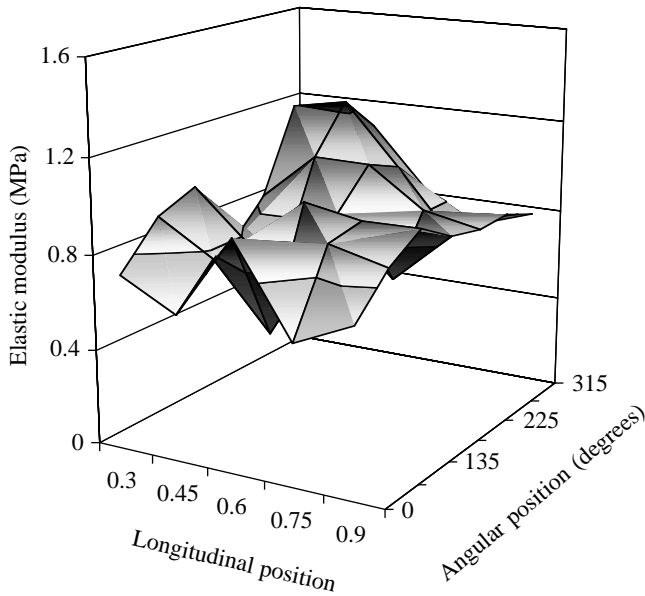


Fig. 5. Elastic modulus values for all 35 mantle positions tested (three trial values for each position were averaged to produce a single value). See Fig. 2 for an explanation of mantle positions. The *x* axis represents the five X<sub>m</sub> positions along the mantle, where X<sub>m</sub> is mantle length, the *y* axis shows the modulus of elasticity, and the *z* axis shows the seven positions around the circumference of each X<sub>m</sub> ring.

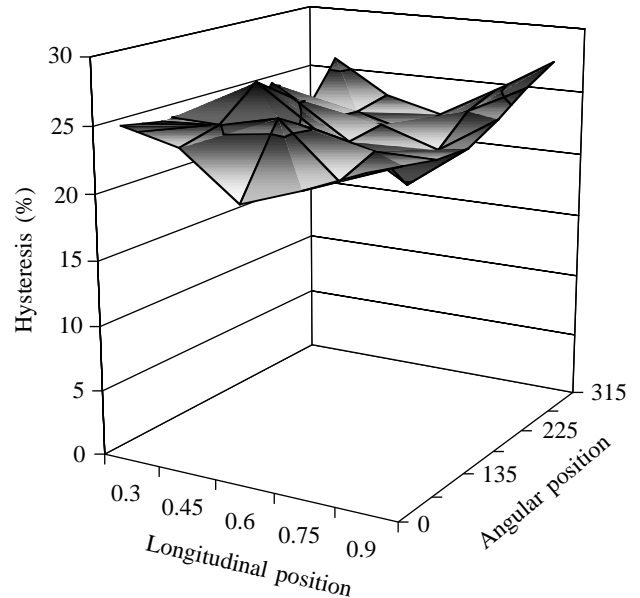


Fig. 6. Hysteresis values for all 35 mantle positions tested (three trial values for each position were averaged to produce a single value). See Fig. 2 for an explanation of mantle positions. The *x* axis represents the five X<sub>m</sub> positions along the mantle, where X<sub>m</sub> is mantle length, the *y* axis shows the hysteresis, and the *z* axis shows the seven positions around the circumference of each X<sub>m</sub> ring.

Table 2. Mean hysteresis (%) for each position on the squid mantle

Ring position	Mantle position					
	0.3 $X_m$	0.45 $X_m$	0.6 $X_m$	0.75 $X_m$	0.9 $X_m$	Mean
0	25.3±0.69	24.2±0.50	20.8±0.55	22.4±0.84	24.2±1.22	23.4
45	24.7±0.64	25±0.95	26±0.80	22±0.48	23.7±1.46	24.3
135	23.9±0.81	27.3±1.03	24.3±0.83	23.2±0.73	23.1±0.49	24.4
180	21.2±0.70	25.3±1.01	22.5±0.60	19.7±0.31	23±0.68	22.4
225	25.2±0.78	22.8±1.34	22.9±0.92	21.4±0.88	24.3±0.63	23.3
270	22±1.06	22.5±0.54	21.4±0.68	23.6±1.1	25.9±1.3	23.1
315	25.8±0.72	23.1±0.73	22±0.62	24.5±1.68	27.2±1.02	24.5
Mean	24.0	24.3	22.8	22.4	24.5	

Mantle positions are defined in Fig. 2;  $X_m$ , mantle length. Values are means  $\pm$  S.E.M. ( $N=15$ ).

five  $X_m$  mantle positions. The maximum *in vivo* circumferential strains used were taken from Fig. 7. Two separate sets of calculations were made by the program, one using the mean peak strains for the slow-swimming squid and

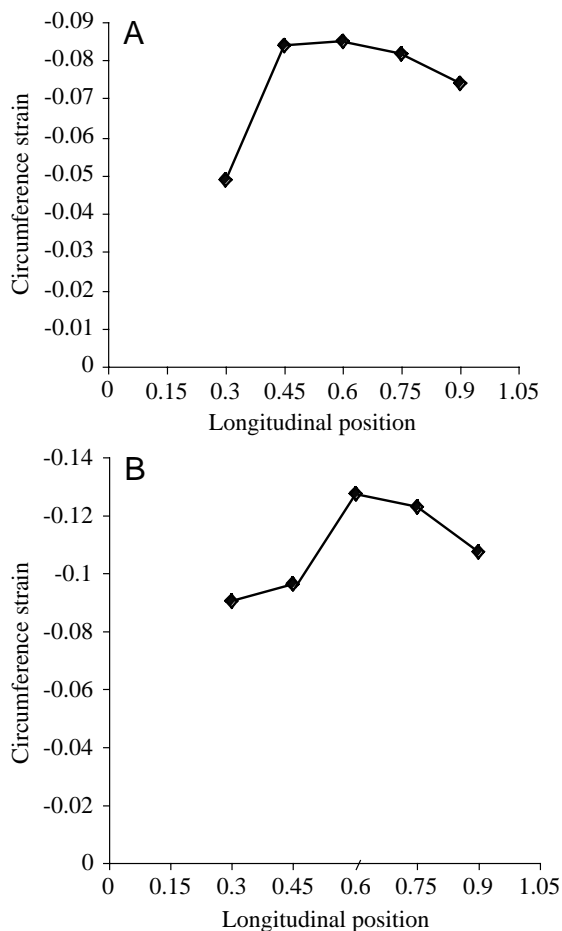


Fig. 7. (A) *In vivo* circumferential strain data for the slow-swimming squid travelling at a velocity  $V$  of  $25.04 \text{ cm s}^{-1}$ . (B) Mean *in vivo* circumferential strain data for the two fast-swimming squid ( $V_{\text{avg}} = 38.5 \text{ cm s}^{-1}$ ). Longitudinal position is expressed as a proportion of mantle length  $X_m$ .

one using the mean peak strains for the fast-swimming squid. Each energy per unit volume value for the corresponding  $X_m$  position for both slow-swimming and fast-swimming squid was then multiplied by the mean sample thickness ( $t$ ) and  $1 \text{ mm} \times 1 \text{ mm}$  (an arbitrarily chosen area) for each of the 35 positions to give the absolute energy storage (in J) in a volume of tissue  $1 \text{ mm} \times 1 \text{ mm} \times t$  from that particular position for that particular swimming speed. This provided an absolute energy storage distribution over the entire mantle. The absolute energy storage for each of the 35 mantle positions is shown in Fig. 8A for a slow-swimming squid ( $25 \text{ cm s}^{-1}$ ) and in Fig. 8B for the fast-swimming squid ( $38\text{--}39 \text{ cm s}^{-1}$ ).

Fig. 9 shows a series of polarized light micrographs from samples taken along the mantle (0.30 $X_m$  to 0.90 $X_m$ ). The results of the quantitative image analysis are summarized in Tables 3 and 4, which show mantle characteristics to be maximized close to 0.60 $X_m$ . Table 3 shows the mean radial muscle spacing and Table 4 shows the mean percentage of micrograph area occupied by circular muscles for each of the 35 mantle positions.

None of the mantle tissue stained with the modified Weigert's technique. The elastic fibres in the wall of the aorta present in some of the mantle-containing sections stained intensely with the modified Weigert's technique.

Analysis of the fibrous connective tissue elements at the electron microscope level for all three sets of intramuscular fibres (IM-1, IM-2 and IM-3) indicated the presence of collagen fibres  $1.5\text{--}4.5 \mu\text{m}$  in diameter. Representative micrographs are shown in Fig. 10. The fibres are composed of closely packed collagen fibrils,  $20\text{--}26 \text{ nm}$  in diameter, which have indistinct cross striations (Figs 11, 12). Fibrils are aligned laterally to form fibres that vary in shape from being relatively straight with some undulations of the fibrils (Figs 10, 11A) to being wavy and/or coiled with undulations, turning and twisting of the fibrils (Fig. 12).

## Discussion

Most of the properties of the squid mantle tested and quantified in this study have not been investigated previously.

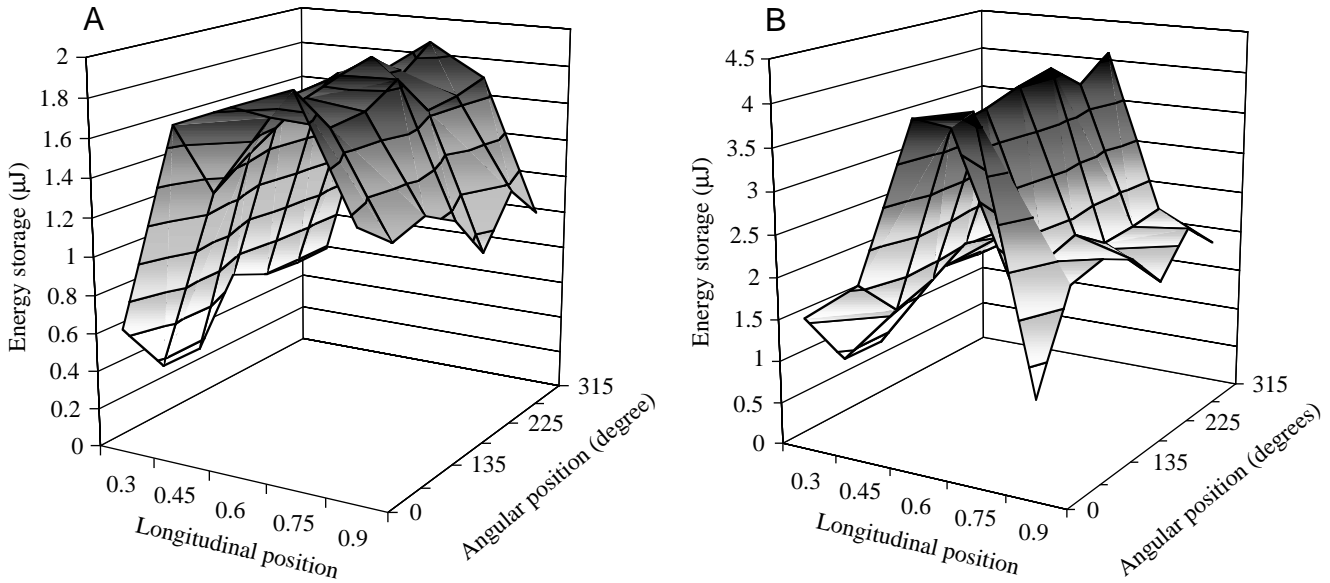


Fig. 8. Absolute energy storage (=energy input) in a piece of mantle tissue 1 mm×1 mm×*t*, where *t* is sample thickness for each of the 35 mantle positions in the slow-swimming ( $V=25.04 \text{ cms}^{-1}$ ) squid (A) and the two fast-swimming ( $V_{\text{avg}}=38.5 \text{ cms}^{-1}$ ) squid (B). Note that the averaged strain data for the two fast-swimming squid were used in the calculation for B. The *x* axis represents the five  $X_m$  positions along the mantle, where  $X_m$  is mantle length, the *y* axis shows the energy storage ( $\mu\text{J}$ ), and the *z* axis shows the seven positions around the circumference of each  $X_m$  ring. See Fig. 2 for an explanation of mantle positions.

Table 3. Mean radial muscle spacing ( $\mu\text{m}$ ) for each position on the squid mantle

Ring position	Mantle position					Mean
	0.3 $X_m$	0.45 $X_m$	0.6 $X_m$	0.75 $X_m$	0.9 $X_m$	
0	486±10.0	515±39.8	561±83.4	420±34.2	350±13.3	467
45	419±6.8	453±28.0	570±9.3	424±0.2	285±16.3	431
135	412±17.4	466±44.2	591±115.2	400±43.4	225±0.9	419
180	250±69.1	522±79.7	443±15.0	338±13.3	204±17.7	352
225	256±51.3	451±1.2	547±18.1	366±15.4	206±10.5	366
270	370±1.9	342±64.7	374±103.8	286±12.5	136±3.8	302
315	402±2.5	582±37.4	455±60.4	344±19.7	212±0.6	399
Mean	371	476	506	369	232	

Mantle positions are defined in Fig. 2;  $X_m$ , mantle length.  
 Values are means ± S.E.M. ( $N=2$ ).

Table 4. Mean percentage of micrograph area occupied by circular muscles for each position on the squid mantle

Ring position	Mantle position					Mean
	0.3 $X_m$	0.45 $X_m$	0.6 $X_m$	0.75 $X_m$	0.9 $X_m$	
0	91.3±0.8	92.4±1.5	94.4±0.6	92.6±0.4	92±1.4	92.5
45	91.9±0.2	91.7±0.1	92±0.3	93.1±1.1	89.8±0.7	91.7
135	91.4±0.3	93.3±0.4	92.3±0.3	93.1±0.7	90.6±0.5	92.1
180	90.7±0.5	93±2.0	92.5±0.3	92.1±0.3	91.7±0.9	92.0
225	93±0.3	92±0.1	93.3±1.6	91.9±0.3	85.6±0.04	91.2
270	92.1±1.1	93.4±0.2	93.2±0.04	92±0.3	84.1±0.1	91.0
315	94±1.1	94±0.2	92.3±0.3	92.6±1.8	89.1±0.5	92.4
Mean	92.0	92.8	92.9	92.5	89.0	

Mantle positions are defined in Fig. 2;  $X_m$ , mantle length.  
 Values are means ± S.E.M. ( $N=2$ ).

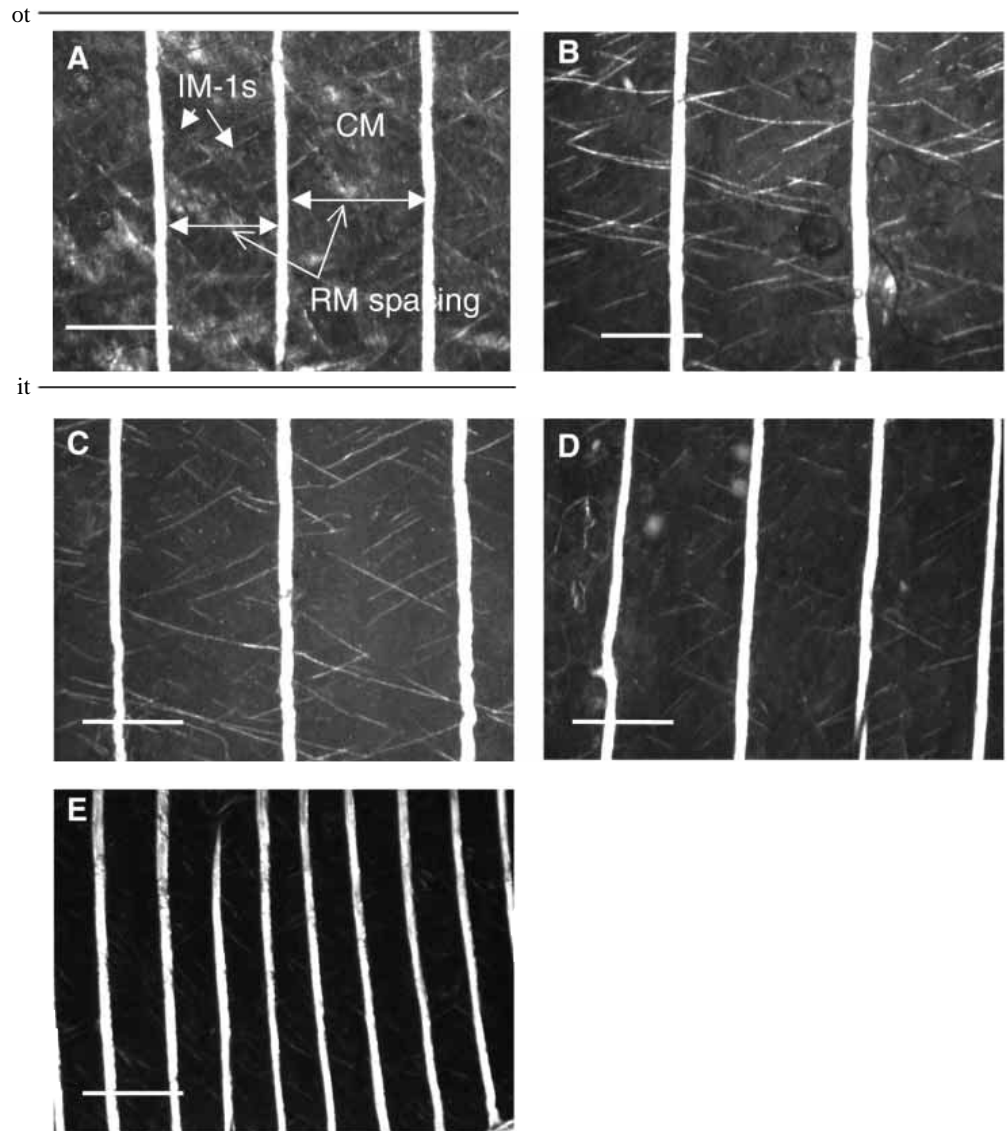


Fig. 9. Polarized light micrographs of squid mantle showing the change in muscle arrangement along the mantle. The outer tunic (ot) and inner tunic (it) positions are not to scale. On average, 4–6 micrographs of this height would be needed to traverse the mantle. All the micrographs shown were taken of the mantle tissue in the centre of the mantle (i.e. approximately equidistant from the inner and outer tunics). RM, radial muscle; CM, circular muscle; IM-1s, intramuscular fibres of set 1. (A) Sample location  $0.30X_m$ ,  $315^\circ$ ; (B) sample location  $0.45X_m$ ,  $315^\circ$ ; (C) sample location  $0.60X_m$ ,  $225^\circ$ ; (D) sample location  $0.75X_m$ ,  $315^\circ$ ; (E) sample location  $0.90X_m$ ,  $270^\circ$ .  $X_m$ , mantle length. See Fig. 2 for an explanation of sample locations. Bars,  $400\mu\text{m}$ .

Gosline and Shadwick (1983a), however, made a single estimate of the modulus and hysteresis of a randomly selected tissue block from a *Loligo opalescens* specimen. They report a modulus of elasticity of  $2 \times 10^6 \text{ N m}^{-2}$  and a hysteresis of approximately 25–30%. The modulus results from the present study indicate that the mean values for each of the 35 positions ranged from  $5 \times 10^5$  to  $1.2 \times 10^6 \text{ N m}^{-2}$ , with an overall mean of  $8.5 \times 10^5 \text{ N m}^{-2}$ , significantly less than that stated by Gosline and Shadwick (1983a). It should be noted, however, that Gosline and Shadwick (1983a) measured the elastic modulus between strains of  $-0.25$  and  $-0.35$ , a range much higher than the *in vivo* strain range we recorded for casual jetting and that we predicted for escape jetting ( $-0.15$  to  $-0.20$ ). In the light of this, it is no surprise that we report an elastic modulus significantly lower than the  $2.0 \times 10^6 \text{ N m}^{-2}$  of Gosline and Shadwick (1983a). The latter value was also determined for a different species *Loligo opalescens*, whereas the focus of the present study was *Loligo pealei*.

There have been relatively few comparative studies concentrating on the mantle characteristics of different squid. Bone et al. (1981) describe the organization of the mantle musculature in the squid *Alloteuthis subulata* and, in lesser depth, the mantles of *Loligo forbesi* and *Sepia officinalis*. They found that the organization of muscle was essentially the same among all three species. Mommsen et al. (1981), after examining five species of squid (each representative of a different genus), found evidence of metabolic differentiation of the mantle musculature. Both these studies imply that the mantle musculature of squid of the same genus (in this case *Loligo*) is organised similarly as a result of their taxonomic association.

The extensive statistical analysis carried out in the present study revealed no discernible patterns between the elastic modulus and any variable tested and, most importantly, showed no significant patterns of change either along or around the mantle. Thus, the modulus of elasticity has been shown to vary within a narrow range and in no predictable manner.

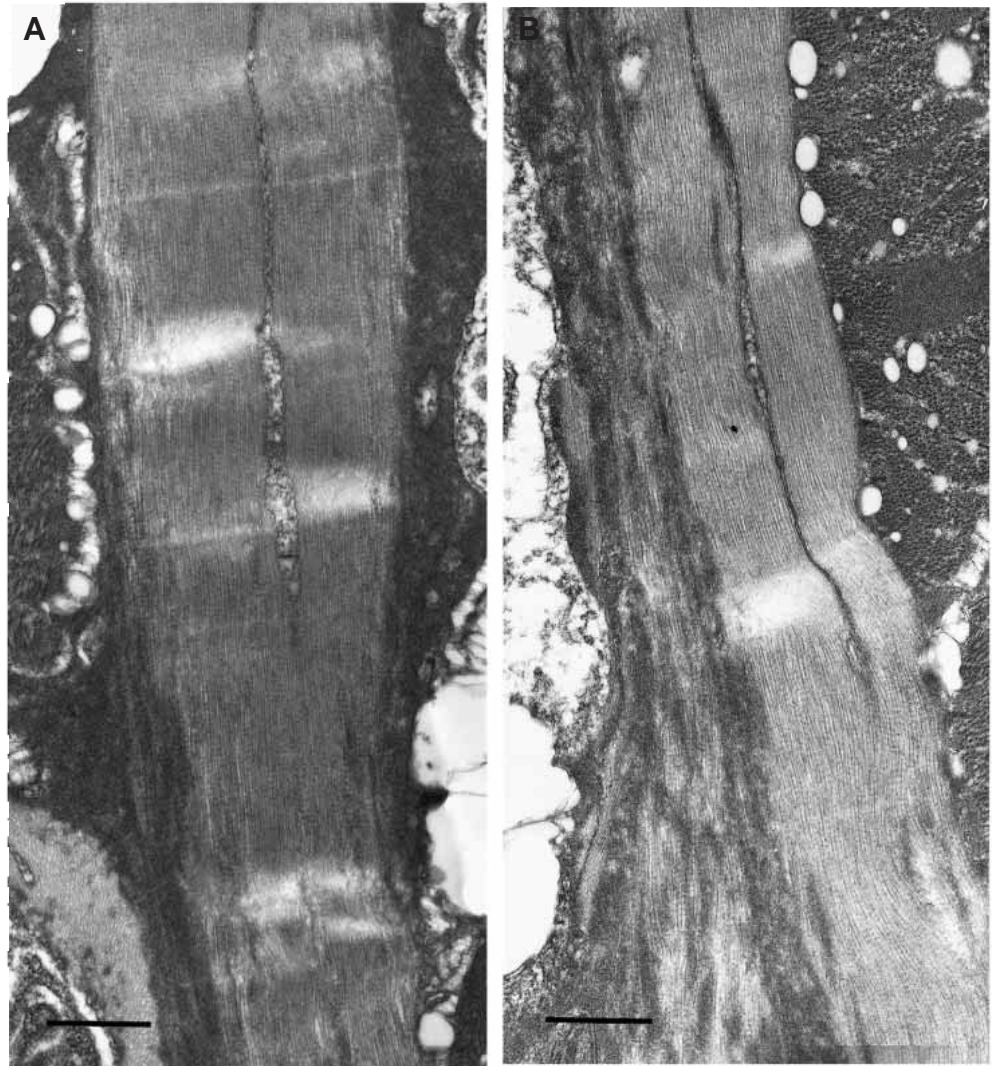


Fig. 10. (A,B) Representative electron micrographs of the intramuscular fibres of the mantle indicating the presence of collagen fibres 1.5–4.5  $\mu\text{m}$  in diameter. Scale bars, 1  $\mu\text{m}$ .

A very similar conclusion was found for the hysteresis results. The statistical analysis showed no discernible patterns between the hysteresis and any variables tested and, as with the modulus, showed no significant patterns either along or around the mantle. The mean hysteresis values for each mantle position were similar to the value of 25% reported by Gosline and Shadwick (1983a) for *L. opalescens*, ranging from 19.7% to 27.3% with an overall mean of 23.6%.

The *in vivo* mantle strains of a jetting squid mantle were quantified in the present study. In both slow- and fast-swimming squid, the strains peak in the middle of the mantle ( $0.60X_m$ ) and decline at either end (Fig. 7). It is important to emphasize that strain is normalized deformation, meaning there is a greater percentage change in thickness of the mantle tissue in the middle compared with the anterior or posterior regions in addition to the greater absolute magnitude of deformation in the middle expected from the larger mantle diameter in this region. This trend in strain will be related to the microscopic structure of the mantle later in the Discussion.

Another very important observation is that the strains increase dramatically when the squid increases its swimming velocity. The maximum strain in the slow-swimming squid was 8.49% while in the fast-swimming squid it is 12.72%, an increase of 4.23%. This indicates that, as the frequency of contraction increases, the magnitude of contraction tends to increase as well. Thus, as the squid swims at a higher frequency, it contracts either a greater proportion of its slow-twitch circular muscles or contracts them to a greater extent with each contraction, or both of these. This suggestion agrees with the previous proposal (Gosline et al., 1983) that a certain amount of variation in the 'basic' pattern of jetting is likely, resulting from the highly developed, complex nervous system (Wells, 1978) of the squid which probably enables it to use several different patterns of muscle activity in both 'casual' and 'escape-jet' swimming depending on the activity and preferred velocity.

Quantification of *in vivo* strains enabled estimates of the energy storage of mantle tissue for all 35 positions tested. It was assumed that the strain was constant around each  $X_m$  ring,

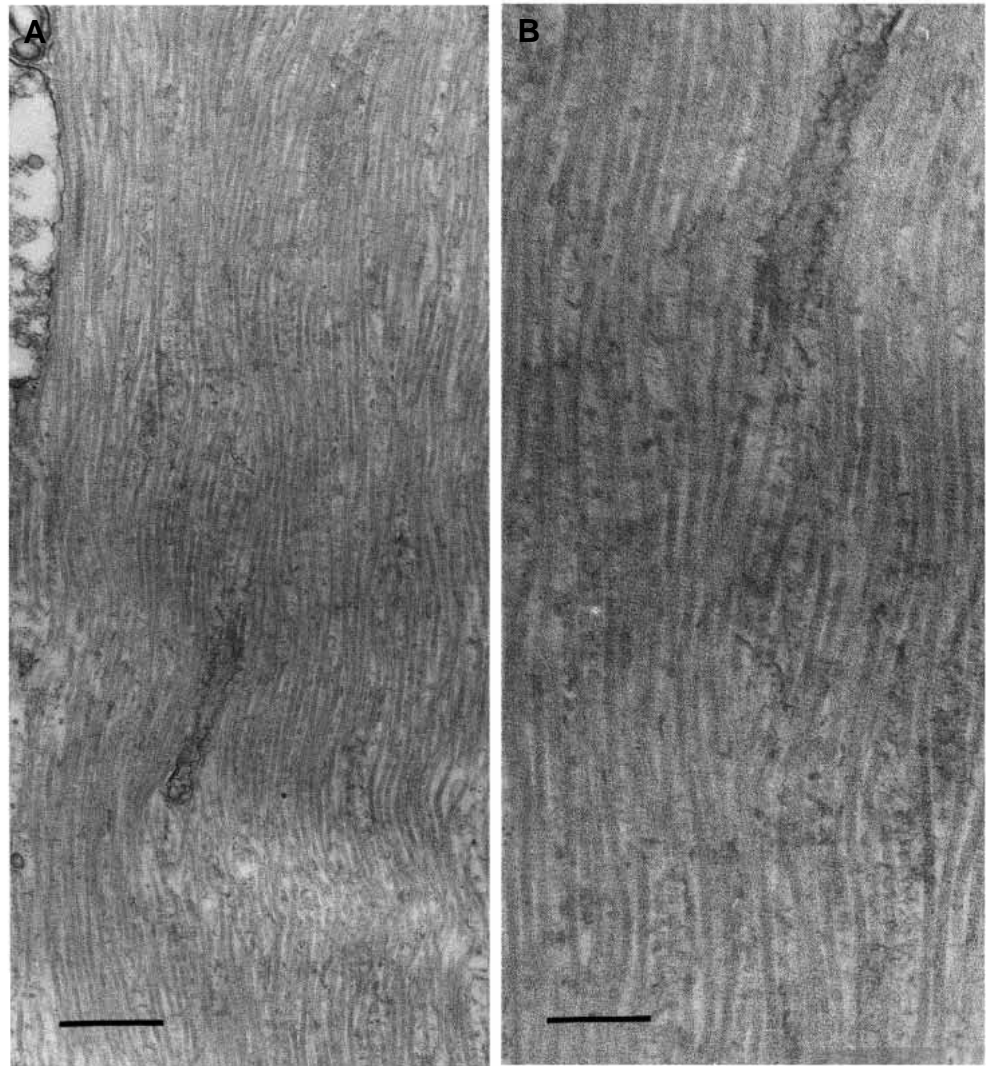


Fig. 11. (A,B) High magnifications of collagen fibres (mantle intramuscular fibres) showing that they are made up of tightly packed collagen fibrils which have indistinct cross striations. (A) Scale bar, 400 nm. (B) Scale bar, 198 nm.

although the ventral ( $180\text{--}360^\circ$ , see Fig. 2) region may inherently have a potential for higher strains than the dorsal region, which may be restricted by the rigid chitinous pen that serves as the mantle scaffolding. The clear pattern found for energy storage (Fig. 8) shows that most of the energy is stored in the same region where the mantle strains are maximized; the middle of the mantle (approximately  $0.60X_m$ ). There are two main contributing factors which explain this trend in energy storage. First, higher strains in the middle of the mantle result in greater tissue deformation and thus more energy being stored in the intramuscular fibres (IM-1 and IM-2). Second, the mantle tissue is thicker on average in the middle of the mantle than at the anterior and posterior ends. The more tissue that is present the more energy-storing fibres there are, and the more energy will be stored and returned.

Energy storage increases as the swimming velocity increases (Fig. 7). This makes sense in the light of the increased strains that occur with increasing velocity. When the squid increases its velocity from  $25\text{ cm s}^{-1}$  to  $38.5\text{ cm s}^{-1}$ , the energy stored more than doubles.

These energy calculations give the energy stored per unit volume. These data can be used to estimate the total energy stored during a contraction, which can be compared with the energy required to produce a jet. The energy stored per unit volume in the mantle of a slow-swimming squid is approximately  $440\text{ J m}^{-3}$ . The maximum volume of a typical squid ( $X_m=23\text{ cm}$ ) can be estimated as  $9\times 10^{-5}\text{ m}^3$  by assuming a cylindrical geometry. This gives a total maximum energy storage during a contraction of approximately 40 mJ. The amount of energy recovered is approximately 30 mJ (using a hysteresis of approximately 25%). Thus, the total cost of mantle deformation for a jet cycle is  $40-30=10\text{ mJ}$ . For comparison, the minimum energy required to produce a jet for a similar-sized slow-moving squid is 12 mJ (Anderson, 1998). Thus, the cost of deforming the mantle is a significant proportion of the cost of producing the jet. We are presently correlating these mantle mechanical properties with the *in vivo* pressure distribution on the swimming squid.

A number of trends in the measured morphological characters were noted from the polarized light micrograph

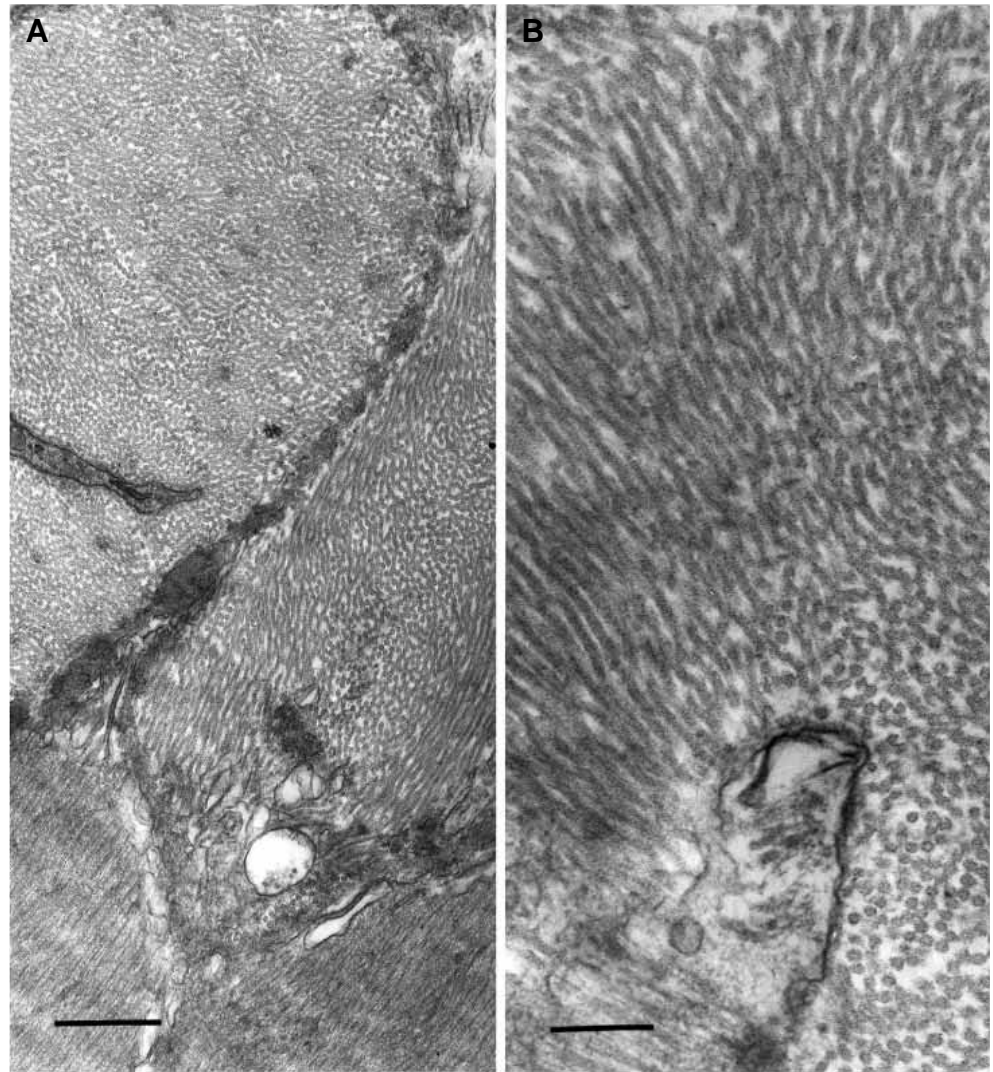


Fig. 12. High magnifications of collagen fibrils making up the intramuscular fibres of the mantle. Fibrils are aligned laterally to form fibres that vary in shape from being relatively straight with some undulations of the fibrils to being wavy and/or coiled with many undulations, turning and twisting of the fibrils. (A) Two adjacent fibres (groups of fibrils) showing fibrils in cross and longitudinal section. Scale bar, 486 nm. (B) Higher magnification showing the twisting nature of the fibrils. Scale bar, 198 nm.

analysis. The obvious trend is along the mantle, but there are some very interesting changes around the mantle as well. The mean radial muscle spacing and, conversely, circular muscle thickness (since radial muscle spacing remains approximately constant from the inner to outer tunic, this thickness applies to both slow- and fast-twitch circular muscle) are low at  $0.30X_m$ , greater at  $0.45X_m$  and peak at  $0.60X_m$ , approximately the middle of the mantle (Table 3). Towards the anterior end of the mantle, the radial muscle spacing decreases again reaching a minimum at  $0.90X_m$ . Thus, radial muscle spacing and circular muscle thickness follow a clear pattern with minimum values at the anterior and posterior ends and a maximum in the middle of the mantle. This trend in the microscopic structure corresponds exactly with the patterns observed for *in vivo* strains and energy storage. Initially, it appears that these macroscopic trends could be attributed to the greater thickness of circular muscle present in the middle than at the ends of the mantle. However, when the percentage of micrograph area occupied by the circular muscles was determined at each position along the mantle (Table 4), this value showed very

little variation except possibly at the extreme anterior end ( $0.90X_m$ ) of the mantle where there is a tendency for the percentage to decrease. This indicates that relatively the same amount of circular muscle is found along most of the mantle. What appears to be occurring is that, although the relative amounts of circular and radial muscles remain constant, the arrangement (number) and thickness of the muscles varies dramatically in a similar manner to the trends found for the *in vivo* mantle strains and *in vivo* energy storage. The fact that these microscopic mantle tissue characteristics correlate so well with the macroscopic properties investigated strongly suggests some linkage between the two. An exact explanation of the correlation is not available, but an investigation presently under way into the muscle architecture of squid may yield possible solutions.

Another interesting observation from the micrographs is that the angle of the IM-1 fibres in longitudinal section (Fig. 9) seems to vary along and possibly even around the mantle, not being restricted to the  $30^\circ$  measured by Ward and Wainwright (1972) and Gosline and Shadwick (1983a). Further quantitative

image analysis should lead to a thorough description of this IM-1 fibre angle distribution.

As with the trends found along the mantle length, the pattern that was noted around the mantle circumference does not involve changes in the relative amounts of circular and radial muscles, but rather involves changes in the arrangement and thickness of these tissues. The data suggest that, as one moves from the dorsal section (45°, 135°, see Fig. 2) of the mantle to the ventral section (225°, 270°, 315°), the number of radial muscles increases (Table 3) as the circular muscle thickness and radial muscle thickness decrease. The most dramatic increase in the number of radial muscles occurs for the most ventral point in the mantle, 270°. This pattern suggests that the arrangement of muscles is adapted to the distribution of stress around the mantle. Consequently, further work on squid mantle tissue will investigate how the muscle architecture correlates with the stress distribution around and along the mantle.

Finally, the present study has resolved the composition of the three different IM fibre types. Gosline and Shadwick (1983a) suggested previously that all three sets of IM fibres were collagenous on the basis of the birefringence of IM-1 fibres, the angle of these fibres through the mantle, and a mantle (not including the collagenous tunic) collagen content of 1%. We found no staining with the modified Weigert's technique, suggesting that no elastic-tissue-associated fibres (elastic, elaunin and oxytalan) were present in the mantle. Furthermore, electron microscopy (Fig. 10) indicated that all three sets of intramuscular fibres were collagen fibres 1.5–4.5 µm in diameter. These fibres varied in shape and direction.

The present study has revealed information about the structure, mechanics and energetics of the squid mantle that will, in combination with our future fluid-dynamic work on the squid, provide a complete description of all *in vivo* forces on a swimming squid. This research may give some useful insights into the tissue mechanics of the squid and may initiate other more complete tissue analyses that look at entire locomotory systems as opposed to isolated or random regions alone. In the light of this, studies of some other elastic systems, such as the vertebrate heart (Robinson et al., 1986), may benefit immensely by approaching them as systems of optimization as well as integration.

This work was funded by an NSERC (Canada) grant to M.E.D., who also received support from the Ester A. and Joseph Klingstein fund from the Marine Biological Laboratory (MBL, Woods Hole). P.S.M. was supported by an NSERC Undergraduate Summer Research Scholarship. We thank R. Hanlon and M. Maxwell at MBL and S. Gallager at the Woods Hole Oceanographic Institute. We also thank R.

Bland (St Francis Xavier University), and D. Wadowska (University of Prince Edward Island) for their technical assistance.

## References

- Aaron, B. B. and Gosline, J. M.** (1980). Optical properties of single elastin fibres indicate random protein conformation. *Nature* **287**, 865–867.
- Anderson, E. J.** (1998). The mechanics of squid locomotion. MSc thesis, St Francis Xavier University, Antigonish, Nova Scotia, Canada.
- Bone, Q., Pulsford, A. and Chubb, A. D.** (1981). Squid mantle muscle. *J. Mar. Biol. Ass. U.K.* **61**, 327–342.
- Cheng, J.-Y., Davidson, I. G. and DeMont, M. E.** (1996). Dynamics and energetics of scallop locomotion. *J. Exp. Biol.* **199**, 1931–1946.
- Cheng, J.-Y. and DeMont, M. E.** (1996a). Hydrodynamics of scallop locomotion: unsteady fluid forces on clapping shells. *J. Fluid Mech.* **317**, 73–90.
- Cheng, J.-Y. and DeMont, M. E.** (1996b). Jet propelled swimming in scallops: swimming mechanics and ontogenetic scaling. *Can. J. Zool.* **74**, 1734–1748.
- Cheng, J.-Y. and DeMont, M. E.** (1997). A predicted *in vivo* muscle force–velocity trajectory. *Can. J. Zool.* **75**, 371–375.
- Davidson, I. G., Wright, G. M. and DeMont, M. E.** (1995). The structure and physical properties of invertebrate and primitive vertebrate arteries. *J. Exp. Biol.* **198**, 2185–2196.
- Gosline, J. M. and DeMont, M. E.** (1985). Jet-propelled swimming in squids. *Scient. Am.* **252**, 96–103.
- Gosline, J. M. and Shadwick, R. E.** (1983a). Molluscan collagen and its mechanical organization in squid mantle. In *Biochemistry of Mollusca* (ed. P. W. Hochachka), pp. 371–398. New York: Academic Press.
- Gosline, J. M. and Shadwick, R. E.** (1983b). The role of elastic energy storage mechanisms in swimming: an analysis of mantle elasticity in escape jetting in the squid, *Loligo opalescens*. *Can. J. Zool.* **61**, 1421–1431.
- Gosline, J. M., Steeves, J. D., Harman, A. D. and DeMont, M. E.** (1983). Patterns of circular and radial mantle muscle activity in respiratory and jetting of the squid *Loligo opalescens*. *J. Exp. Biol.* **104**, 97–109.
- Mommsen, T. P., Ballantyne, J., MacDonald, D., Gosline, J. and Hochachka, P. W.** (1981). Analogues of red and white muscle in squid mantle. *Proc. Natl. Acad. Sci. USA* **78**, 3274–3278.
- Montes, G. S.** (1992). Distribution of oxytalan, elaunin and elastic fibres in tissues. *J. Brazilian Ass. Adv. Sci.* **44**, 224–233.
- Robinson, T. F., Factor, S. M. and Sonnenblick, E. H.** (1986). The heart as a suction pump. *Scient. Am.* **254**, 84–91.
- Ward, D. V. and Wainwright, S. A.** (1972). Locomotory aspects of squid mantle structure. *J. Zool., Lond.* **167**, 437–449.
- Wells, M. J.** (1978). *Octopus*. London: Chapman & Hall. 417pp.
- Winkelmann, R. K. and Schmitt, R. W.** (1957). A simple silver method for nerve axoplasm. *Proc. Mayo Clinic* **32**, 217–222.